PCCP

ROYAL SOCIETY OF CHEMISTRY

PAPER

View Article Online
View Journal | View Issue

Cite this: *Phys. Chem. Chem. Phys.*, 2020, **22**, 24257

Diagonal Born–Oppenheimer corrections to the ground electronic state potential energy surfaces of ozone: improvement of *ab initio* vibrational band centers for the $^{16}O_3$, $^{17}O_3$ and $^{18}O_3$ isotopologues†

Attila Tajti, *[a] Péter G. Szalay, [a] Roman Kochanov [bc] and Vladimir G. Tyuterev *[bd]

Mass-dependent diagonal Born–Oppenheimer corrections (DBOCs) to the *ab initio* electronic ground state potential energy surface for the main $^{16}O_3$ isotopologue and for homogeneous isotopic substitutions $^{17}O_3$ and $^{18}O_3$ of the ozone molecule are reported for the first time. The system being of strongly multiconfigurational character, multireference configuration interaction wave function ansatz with different complete active spaces was used. The reliable DBOC calculations with the targeted accuracy were possible to carry out up to about half of the dissociation threshold D_0. The comparison with the experimental band centers shows a significant improvement of the accuracy with respect to the best Born–Oppenheimer (BO) *ab initio* calculations reducing the total root-mean-squares (calculated–observed) deviations by about a factor of two. For the set of $^{16}O_3$ vibrations up to five bending and four stretching quanta, the mean (calculated–observed) deviations drop down from 0.7 cm^{-1} (BO) to about 0.1 cm^{-1}, with the most pronounced improvement seen for bending states and for mixed bending-stretching polyads. In the case of bending band centers directly observed under high spectral resolutions, the errors are reduced by more than an order of magnitude down to 0.02 cm^{-1} from the observed levels, approaching nearly experimental accuracy. A similar improvement for heavy isotopologues shows that the reported DBOC corrections almost remove the systematic BO errors in vibrational levels below $D_0/2$, though the scatter increases towards higher energies. The possible reasons for this finding, as well as remaining issues are discussed in detail. The reported results provide an encouraging accuracy validation for the multireference methods of the *ab initio* theory. New sets of *ab initio* vibrational states can be used for improving effective spectroscopic models for analyses of the observed high-resolution spectra, particularly in the cases of accidental resonances with "dark" states requiring accurate theoretical predictions.

Received 6th May 2020,
Accepted 31st August 2020

DOI: 10.1039/d0cp02457k

rsc.li/pccp

1 Introduction

Accurate potential energy surfaces (PESs) as a function of the nuclear coordinates are prerequisites for reliable theoretical studies of molecular spectroscopy and dynamics. Precise knowledge of vibrational spectra of the ozone molecule is mandatory for spectral analyses because of its importance for atmospheric applications.[1–4] Since early *ab initio* works,[5–7] it has been recognized that the ozone molecule possesses quite a complicated electronic structure[1,8–11] attracting much attention for the study of both the ground[12–14] and excited electronic states.[15] On the experimental side, the incentive for in-depth investigations was related to isotopic anomalies in the ozone formation discovered both in the atmosphere and in the laboratory settings.[16–21] Over the years this was a motivation for

[a] *ELTE Eötvös Loránd University, Institute of Chemistry, Laboratory of Theoretical Chemistry, P. O. Box 32, H-1518, Budapest 112, Hungary. E-mail: tat@chem.elte.hu*
[b] *Tomsk State Research University, Laboratory of Quantum Mechanics and Radiative Processes, Russia*
[c] *V.E. Zuev Institute of Atmospheric Optics, Russian Academy of Sciences, Laboratory of Theoretical Spectroscopy, Tomsk, Russia*
[d] *Université de Reims, Groupe de Spectrométrie Moléculaire et Atmosphérique, France. E-mail: vladimir.tyuterev@univ-reims.fr*

† Electronic supplementary information (ESI) available: The Python codes for the analytical DBOC representations for each investigated isotopologue and comparisons for the calculated and observed vibrational energies. See DOI: 10.1039/d0cp02457k

many studies of vibrational energy patterns,[12,22–24] infrared spectra of ozone isotopologues (see ref. 24–31, and references therein) and for the dynamics of isotopic exchange reactions.[32–38] The non-adiabatic coupling of the electronic states has been discussed in ref. 39 and 40. However, to our knowledge, all available full-dimensional PESs of the ozone molecule[1,12–14] have been computed within the framework of the Born–Oppenheimer approximation. The present work aims at the first *ab initio* calculation of the mass-dependent diagonal Born–Oppenheimer corrections (DBOCs) for the 3-dimensional ozone PES and its use in the calculation of vibrational band centers of the $^{16}O_3$, $^{17}O_3$ and $^{18}O_3$ isotopic species. We show that these contributions permit a significant improvement of vibrational calculations with respect to the most accurate available BO surface.

The paper is structured as follows. The ansatz of DBOC calculations, the wave function model for ozone DBOC and the corresponding computational methodology are described in Section 2. The analytic PES model used for the fit of DBOC electronic energy corrections in terms of nuclear geometries is discussed in Section 3. The subsequent Sections 4 and 5 are devoted to a detailed study of the mass-dependent corrections to vibrational states of the $^{16}O_3$, $^{17}O_3$ and $^{18}O_3$ isotopologues and a comparison to experimental data with the conclusions and discussions in Section 6.

2 *Ab initio* calculations

2.1 Diagonal Born–Oppenheimer correction

The diagonal Born–Oppenheimer correction (DBOC) is the leading correction term to the Born–Oppenheimer approximation (BOA) first given by Born and Huang:[41]

$$\begin{aligned}\Delta E_{\mathrm{DBOC}}(\mathbf{R}) &= \langle \Psi(\mathbf{r};\mathbf{R})|\hat{T}_{\mathrm{N}}(\mathbf{R})|\Psi(\mathbf{r};\mathbf{R})\rangle \\ &= \int \Psi^*(\mathbf{r};\mathbf{R})\hat{T}_{\mathrm{N}}(\mathbf{R})\Psi(\mathbf{r};\mathbf{R})\mathrm{d}\mathbf{r},\end{aligned} \tag{1}$$

with Ψ denoting the normalized electronic wave function obtained within the BOA, and $\hat{T}_{\mathrm{N}}$ being the nuclear kinetic energy operator. The integration in eqn (1) is done over all electronic coordinates represented by **r**. The DBOC thus takes into account the dependence of the electronic wave function on the nuclear coordinates **R**, through the calculation of the nuclear kinetic energy contribution. It has the advantage that the adiabatic picture of the BOA is retained so that the notion of a potential energy surface (PES) is still possible. However, the PES becomes dependent on the nuclear mass and will thus be different for, *e.g.* various isotopologues of the same molecule.

The *ab initio* calculation of ΔE_{DBOC} is possible with analytic derivative techniques. Following the pioneering work of Sellers and Pulay[42] and Handy *et al.*[43] who first presented a formula for the evaluation of ΔE_{DBOC} at the Hartree–Fock self-consistent field (HF-SCF) level, several implementations were reported for correlated electronic wave functions.[44–52] The work by some of the present authors,[51] for the first time, made it possible to calculate ΔE_{DBOC} at various levels of configuration interaction (CI) and coupled cluster (CC) theories *via* analytic techniques. The implementation of their formulae for the single-reference coupled cluster singles and doubles (CCSD) and configuration interaction singles and doubles (CISD) models, as well as for the Møllet–Plesset perturbation theory are available today in the CFOUR[53] program. Using an interface to the MRCC[54] program system, calculation of ΔE_{DBOC} is possible not only at any truncation level of single-reference CC and CI theories, but also for various multiconfigurational CI and CC models.[55–58] The evaluation of ΔE_{DBOC} requires the explicit calculation of first order wave function response parameters with respect to nuclear coordinates, and it is thus computationally quite demanding.

The DBOC is often regarded as a predominantly one-electron effect, with the contribution of electron correlation being small, even negligible. However, as shown in ref. 51 and 52, this is not at all the case if accurate energy differences are desired, in which the account of electron correlation contribution in DBOC falls easily in the range of the total DBOC effect. Treating DBOC at correlated levels is thus necessary in studies aiming at subchemical (kJ mol^{-1} or better) accuracy. Fortunately, however, even a relatively low level treatment of dynamic correlation is able to recover a large fraction of the DBOC electron correlation contribution.[52] In terms of the basis set size, it is also shown in ref. 51 that the total DBOC can essentially be considered as converged in triple-ζ quality basis sets, but several wavenumbers away from the basis set limit at the double-ζ level. The DBOC corrections have been included in accurate PES calculations for several molecules (see ref. 47, 59–64 and references therein); however, to our knowledge have never been accounted for the ozone molecule.

2.2 Wave function model for ozone DBOC

In the case of ozone, the complexity of the electronic structure makes the use of a multiconfigurational (MC) wave function model necessary, even in points near the equilibrium structure.[1,9,10,12] The key step in these calculations is the choice of the reference space, which is in most cases a CAS (complete active space) where the "most important" orbitals (the so called active orbitals) are selected and the "most important" electrons (active electrons) are distributed among them. Technically, CAS is denoted by CAS(m,n), where m is the number of active electrons and n is the number of active orbitals. From the chemical point of view, the model that selects all valence orbitals and electrons as active (often referred to as the full-valence CAS space) is a well-defined, unambiguous, and safe choice even for geometries far from the equilibrium. Unfortunately, this often leads to too large ansätze and therefore some simplification is necessary. In the case of ozone, one intends to use the CAS to generate an expansion space by applying single and double excitations to all determinants of the CAS for the treatment of static and dynamic electron correlation in a single wave function model. This can be done *via* a multireference CI singles and doubles (MR-CISD) ansatz in the MRCC program. In the case of the DBOC calculation, the implementation is limited to the use of single-reference HF-SCF orbitals, which represent, beyond the limited size of the CAS, one further compromise to be made. Nevertheless, it is reasonable to assume that the electron correlation effects in

DBOC can still be well recovered, provided that the CAS is constructed properly.

For ozone, performing the MR-CISD DBOC calculations with a full-valence CAS(18,12) space is not possible, at least not in a reasonably sized basis set. In fact, even a CAS(6,6) space is computationally too demanding if, as discussed in Section 2.1, a triple-ζ quality basis set is to be used.

Such challenges are well known in the field of high-accuracy *ab initio* thermochemistry,[65–74] where sub-kJ mol^{-1} accuracy is successfully achieved by considering the effect of higher and higher excitations in the electron correlation treatment *via* energy corrections evaluated in smaller basis sets. This approach, if carried out in the systematic hierarchy of the correlation consistent basis sets of Dunning and co-workers,[75–77] was found to work very well not just for contributions to the total energy, but also to structural and spectroscopic parameters.[69,74,78] Going along this path with the DBOC surface for ozone, we define the function

$$\begin{aligned}\Delta E^{6,6}_{\mathrm{DBOC}}(\mathbf{R}) :=\ & \Delta E_{\mathrm{DBOC}}(\mathbf{R}, \mathrm{CAS}(4,4), \text{cc-pVTZ}) \\ &+ \left(\Delta E_{\mathrm{DBOC}}(\mathbf{R}, \mathrm{CAS}(6,6), \text{cc-pVDZ}) \right. \\ &- \left. \Delta E_{\mathrm{DBOC}}(\mathbf{R}, \mathrm{CAS}(4,4), \text{cc-pVDZ})\right),\end{aligned} \quad (2)$$

which thus accounts for the errors due to the incompleteness of the CAS(4,4) space with respect to the CAS(6,6) one *via* a correction term evaluated in the smaller cc-pVDZ basis set. The DBOC surface defined by eqn (2) is simply referred to as DBOC(6,6) in the subsequent chapters.

2.3 Computational details

DBOC surfaces described by eqn (2), as well as at the simple CAS(4,4)/cc-pVTZ levels were obtained in a set of points corresponding to the sparser grid of the high-accuracy PES from ref. 12. The calculations were performed with the combination of the CFOUR[53] and MRCC[54] program codes at the MR-CISD level. The CAS(6,6) reference space consisted of the three highest-lying occupied and three lowest-lying unoccupied molecular orbitals of the 2p space (the space of orbitals formed by the 2p atomic orbitals of the oxygen atoms), while in the CAS(4,4) space only the highest- and the lowest-lying two occupied and unoccupied orbitals were included, respectively. Due to the lack of core polarization functions in the cc-pVXZ basis set series, all quantities had to be evaluated with the core electrons excluded from the correlation treatment. All calculations were carried out on the ROMEO 2018 supercomputer facility of the University of Reims Champagne-Ardenne.[79]

3 Fitting the analytic models to *ab initio* DBOC values

The summary of calculated *ab initio* points representing DBOC values at a grid of nuclear geometries for the three symmetric isotopologues of ozone is given in Table 1. Here and below we use the standard convention for abbreviated notations of isotopic species ($^{16}O_3$ = 666, $^{17}O_3$ = 777, and $^{18}O_3$ = 888 as specified in the first column), which is generally used in the spectroscopic literature. The upper panel (A) of the table corresponds to the total set of nuclear geometries including those obtained by permutations of r_1 and r_2 bond distances between the central and terminal oxygen atoms of the ozone molecule. The second column represents the range of the mass-dependent DBOC correction, whereas the range of the Born–Oppenheimer PES values (V_{BO}, ref. 12) corresponding to the grid is given in the fourth column. All energy values for both BO and DBOC are converted to wavenumbers. The number of calculated points is shown in the third column. The last three columns give the extent of the internal bond length (r_1, r_2) and apex angle (α) coordinates. A graphical overview of the DBOC corrections on the full grid is shown in Fig. 1 for the principal ozone isotopologue $^{16}O_3$. Differently colored groups of points correspond to two-dimensional cuts of the full PES for fixed values of the apex angle ranging from 100° to 135°.

Several analytical $\Delta V_{\mathrm{DBOC}}(r_1,r_2,\alpha)$ models involving polynomial, Gaussian, exponential, inverse hyperbolic functions and their combinations were tested to fit *ab initio* DBOC values on the full grid of nuclear displacements. At large nuclear displacements from the equilibrium, erratic deviations were obtained for all models. This erratic behavior of the DBOC PES with (*ab initio* – fit) discrepancies larger than several wavenumbers generally occurred

Table 1 Summary for the calculated DBOC correction at the geometrical grid of *ab initio* points for the $^{16}O_3$, $^{17}O_3$ and $^{18}O_3$ isotopologues of ozone

Isotopologue	ΔE_{DBOC}/cm^{-1}	N_{points}	V_{BO}/cm^{-1}	r_1/a.u.	r_2/a.u.	$\angle_{\mathrm{OOO}}$/deg.
(A) Summary of all *ab initio* points						
666	−2.152 to 10.157	489	0–7030.497	2.2–3.0	2.2–3.0	100–135
777	−2.025 to 9.557					
888	−1.925 to 9.024					
(B) Summary for the points with $V_{\mathrm{BO}} \leq 3000$ cm^{-1}						
666	−1.597 to 5.422	247	0–2992.930	2.2–2.7	2.2–2.7	105–130
777	−1.503 to 5.102					
888	−1.425 to 4.815					
(C) Summary for the points with 3000 cm^{-1} $< V_{\mathrm{BO}} <$ 4300 cm^{-1}						
666	−1.661 to 6.435	71	3030.595–4216.636	2.20–2.80	2.20–2.80	105–130
777	−1.563 to 6.055					
888	−1.477 to 5.710					

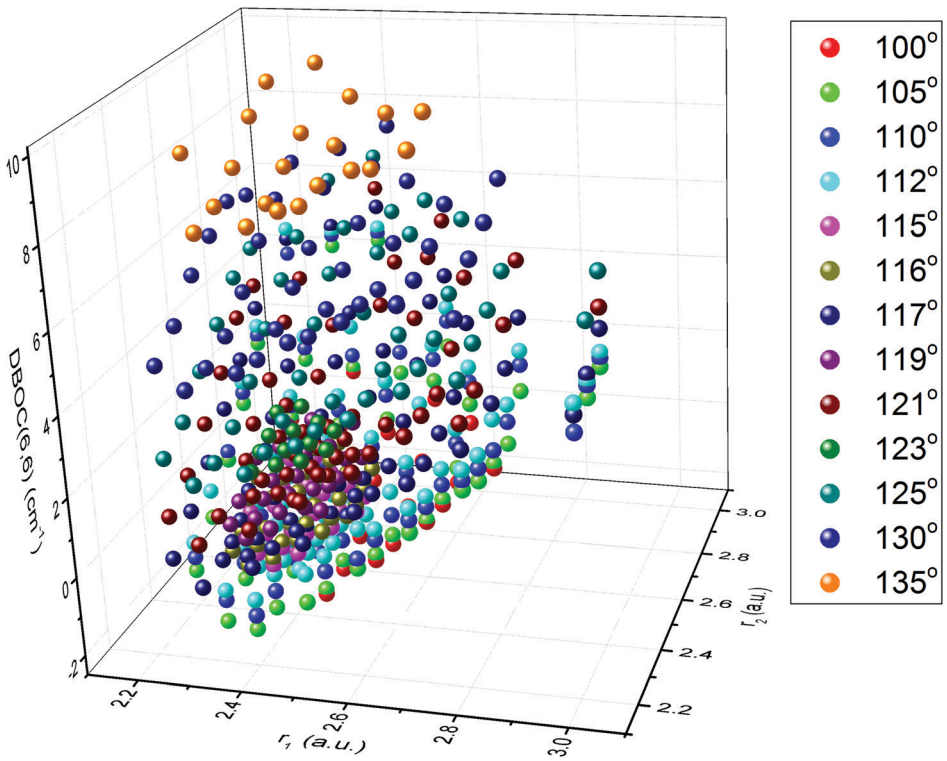

Fig. 1 Overview of the calculated DBOC geometrical grid points for the $^{16}O_3$ isotopologue. The ΔE_{DBOC} values are given in the vertical axis in cm^{-1}. Colors refer to distinct values of the OOO apex angle.

at the energy range above half of the dissociation energy threshold ($D_0/2$), where the experimental value[80,81] of D_0 is about 8560 cm^{-1} (as sited in 9) for the $^{16}O_3$ isotopologue, in terms of the vibrational energy relative to the zero point energy level. Also, for large nuclear displacements corresponding to $V_{BO} > D_0/2$ we have experienced some convergence issues of *ab initio* DBOC calculations, probably to be attributed to the inappropriateness of single-reference HF-SCF orbitals in these structures.

The most accurate to date *ab initio* BO PES constructed by Tyuterev *et al.*[12] provided vibrational level calculations with the root mean square deviation of the calculated and observed values (observed–calculated) of about 0.5 cm^{-1} for low energy vibrations and about 1 cm^{-1} up to 93% of the dissociation threshold D_0. The aim of this work being to improve this accuracy, we focus on the careful investigation of the DBOC corrections at various levels of the theory, at the BO PES range up to 4300 cm^{-1} that roughly corresponds to $D_0/2$. To this end, our grids of points were chosen significantly denser at the bottom of the potential well near the C_{2v} equilibrium (open geometrical configuration of the ozone molecule). Panels (B) and (C) of Table 1 give the corresponding information for the grids below 3000 cm^{-1} and between 3000 cm^{-1} and 4300 cm^{-1}, respectively. In the weighted fit we assigned the largest weights to the points of panel (B), with lower weights for the points presented in panel (C), whereas erratic points beyond $D_0/2$ were excluded from the final fit. Different analytical models gave us quite similar corrections to vibrational levels in this energy range. The final fits were performed with the following analytical form:

$$\Delta V_{DBOC}(r_1, r_2, \alpha) = \left[C - a\mathrm{Exp}\left[-b\left(\left(\frac{r_1}{r_e}-1\right)^2 + \left(\frac{r_2}{r_e}-1\right)^2 + \left(\frac{\cos\alpha}{\cos\alpha_e}-1\right)^2\right)\right] - \sum_{0\le i+j+k\le n} d_{ijk}\left[(r_1-r_e)^i(r_2-r_e)^j + (r_1-r_e)^j(r_r-r_e)^i\right](\cos\alpha-\cos\alpha_e)^k\right] \times \exp\left[-c\left(\left(\frac{r_1}{r_e}-1\right)^2 + \left(\frac{r_2}{r_e}-1\right)^2 + \left(\frac{\cos\alpha}{\cos\alpha_e}-1\right)^2\right)\right] \quad (3)$$

where r_e and α_e are, respectively, the bond length and angle at the C_{2v} equilibrium structure, while a, b, c, C and d_{ijk} are fitted parameters, and n is the order of the expansion. This functional form accounts for the C_{2v} symmetry of the PES for the considered isotopic species. The schematic behavior of the PES is described by the Gaussian function of r_1, r_2 and $\cos\alpha$, and the finer tuning of the surface is done by means of the symmetrized polynomial part. The asymptotic behavior of the correction is controlled by the "global" Gaussian damping function, which ensures that the correction approaches zero at sufficiently large values of r and α, because we do not have reliable *ab initio* information at these ranges of geometries. In individual points, DBOC values of the symmetric (666, 777 and 888) isotopologues

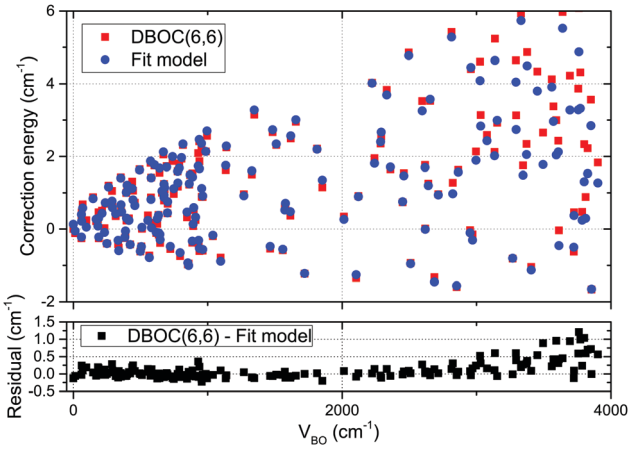

Fig. 2 DBOC values for the geometrical grid points of Fig. 1 (top panel) and fit residuals (bottom panel) for the analytical representation (eqn (3)) plotted for the 666 isotopologue for configurations with potential energy V_{BO} up to 4000 cm^{-1}.

are related to each other *via* a simple scaling factor. Nevertheless, we chose to perform the fit according to eqn (3) separately for the individual symmetric isotopologues, resulting in different, although very similar parameters of the fitted DBOC correction. The final, isotope-dependent PESs were thus then constructed for each isotopologue separately by adding the fitted DBOC surface to the Born–Oppenheimer BO PES[12] in the form

$$V^{(i)}(r_1,r_2,\alpha) = V_{BO}(r_1,r_2,\alpha) + \Delta V^{(i)}_{DBOC}(r_1,r_2,\alpha) \qquad (4)$$

Here (i) denotes one of the 666, 777, and 888 isotopologues. The fitted models were coded in Python and can be found in the ESI.† The residuals of the fit are collected in Fig. 2 for the principal isotopologue and in Table 2 for all three symmetric isotopologues. The deviations of the fit of the analytical ΔV_{DBOC} PES (eqn (3)) to ΔE_{DBOC} values lie mostly within 0.2 cm^{-1} for the configuration energies below 2500 cm^{-1}, and within the 1 cm^{-1} corridor for configurations with energies in the 2500–4300 cm^{-1} range, as shown on the lower panel of Fig. 2.

The behaviour of the DBOC correction with respect to stretching and bending coordinates are, respectively, presented

Table 2 Summary of the fits of the *ab initio* DBOC by the model defined by eqn (4)

Isotopologue	N_{points}	RMS residual/cm^{-1}	Mean residual/cm^{-1}
(A) Total fit summary of the points from (B) and (C) sections			
666	318	0.2892	0.1026
777	318	0.2740	0.0975
888	318	0.2606	0.0928
(B) Fit summary for the points with $E_{BO} \leq 3000$ cm^{-1}			
666	247	0.1039	0.0021
777	247	0.0985	0.0020
888	247	0.0946	0.0019
(C) Fit summary for the points with $3000 < E_{BO} < 4300$ cm^{-1}			
666	71	0.5795	0.4508
777	71	0.5492	0.4284
888	71	0.5217	0.4077

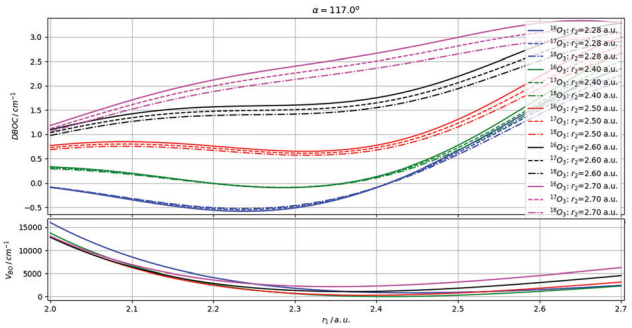

Fig. 3 Fitted DBOC corrections – relative to the equilibrium geometry – along the O–O bond stretching coordinates for the different symmetric isotopologues of ozone.

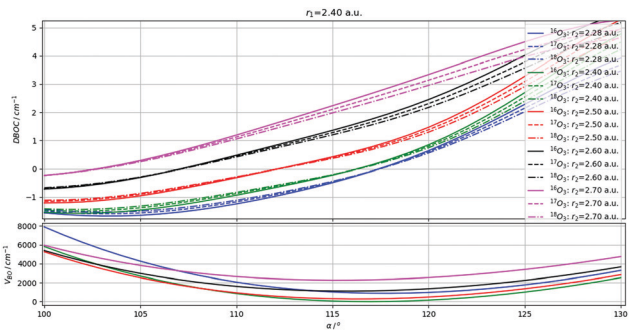

Fig. 4 Fitted DBOC corrections – relative to the equilibrium geometry – along the O–O–O bending coordinate for the different symmetric isotopologues of ozone.

on Fig. 3 and 4. The differences between isotopologues are, as shown by the similarity of the respective curves, very minor. Qualitatively we observe the following properties of the DBOC mass-dependent contributions to the ozone PES. First, they produce somewhat different effects for bond length (stretching) and bond angle (bending) vibrations. The angular dependence of the DBOC correction is quite monotonic, nearly linear in the neighborhood of the BO minimum (Fig. 3). This mainly results in a shift of the equilibrium configuration towards smaller α_e values. On the contrary, the adiabatic correction changes the shape of the PES for the stretching degree of freedom r_1 (Fig. 4), but in a different manner, depending on the instantaneous value of the other bond length r_2. Second, the variation of masses in the case of homogeneous isotopic substitutions 666 → 777 and 666 → 888 produce quite systematic small shifts having nearly the same shape in terms of the coordinate-dependence. It is thus not surprising that DBOC contributions to vibrational levels of $^{16}O_3$, $^{17}O_3$, and $^{18}O_3$, as shown in the next sections, move into the same direction of always being positive.

4 *Ab initio* vibrational energy levels of $^{16}O_3$ with DBOC corrections

Global variational methods permit nowadays converging vibrational basis set calculations to the precision of 0.01 or 0.001 cm^{-1}

for small and medium sized molecules,[12,24,61–64,82–84] at least in the energy range up to the half of the dissociation threshold. This level of precision is necessary for this study to clearly distinguish the contributions beyond the BOA because the best published *ab initio* BO ozone calculations[12,24,85] were already quite accurate with the average (observed–calculated) discrepancies of 0.5 cm^{-1} to 1 cm^{-1}. As often recommended, atomic masses were used for calculations of vibrational levels in order to partly account for non-adiabatic contributions.[86] Considering non-adiabatic contributions at least in this approximate manner seems to be particularly important if the adiabatic correction *via* DBOC is also included. This is due to the fact that if the latter shifts the vibrational levels in the positive direction, the usually negative shift by non-adiabatic effects[87–89] is, at this level of accuracy, required to avoid the general overestimation of the levels. Here vibrational levels were computed in this range using the same variational technique as described in our previous work,[12] the only difference being the inclusion of the mass-dependent DBOC correction to the BO PES according to eqn (4). We consider the effect of vibrational DBOC corrections at two levels of the theory: using complete active spaces CAS(4,4) and CAS(6,6) as described in Section 2. The corresponding results for vibrational levels with the $V_{BO} + \Delta V_{DBOC}$ PESs will be denoted as DBOC(4,4) and DBOC(6,6) for the sake of brevity. The vibrational levels of the ozone molecule are usually assigned in terms of normal mode quantum numbers (v_1, v_2, and v_3) where v_1 stands for symmetric vibration, v_2 for the bending mode and v_3 for the anti-symmetric vibration. Due to molecular symmetry and approximate coincidence of harmonic frequencies ($\omega_1 \approx \omega_3$), they are organized in a series of so called "stretching polyads".[3,22,25] These polyads, denoted as $P_{b,s}$, are defined as sets of nearby vibrational states

$$P_{0,1} = \{(100),(001)\},\ P_{0,2} = \{(200),(101),(002)\},\ldots,$$
$$P_{b,1} = \{(1b0),(0b1)\},\ldots,\ P_{b,s} = \cup\{(v_1 b v_3)\}, \quad (5)$$

where the $\cup$ symbol stands for a union over v_1, and v_3 under the condition that $v_1 + v_3 = s$, which is the total quantum number of stretching vibrations, and $b = v_2$ is the bending quantum number. The intra-polyad couplings among vibrational modes in ozone are dominated by Darling–Dennison resonances and rotation–vibration couplings by Coriolis resonances.[3,25]

It is instructive to investigate the DBOC contributions to individual vibrational levels, as well as to the general polyad-by-polyad picture. An improvement of *ab initio* calculations for vibrational band centers with respect to observations is clearly seen in Tables 3 and 4 where the observed minus calculated discrepancies are collected together with the root-mean-squares (RMS) and mean deviations for various types of polyads. Note that, because of limitations in the construction of accurate DBOC surfaces described in Section 3, all comparisons in this work are given up to energies about $V_{BO} = D_0/2$.

As it is shown in Table 4 and in Fig. 5, the inclusion of DBOC both at the CAS(4,4) and CAS(6,6) levels yields significant improvements with respect to the most accurate available BO calculations,[12] with quite similar results for both active spaces.

The improvement is particularly pronounced for the bending states as follows from the first part of Table 3 and Fig. 7: the (observed–calculated) errors decrease by an order of magnitude when accounting for the DBOC(4,4) or DBOC(6,6) terms in the PES. For the (010), (020) and (030) bending vibrational states the BO + DBOC(6,6) surface provides nearly experimental

Table 3 Comparison of vibrational levels computed from *ab initio* potential energy surfaces at various levels of theory with experimental data for the $^{16}O_3$ ozone isotopologue

T[a]	O = Obs.[b]	($v_1v_2v_3$)[c]	O-BO[d]	O-DBOC(4,4)[e]	O-DBOC(6,6)[e]	Polyad
Bending states						
A	700.93	(010)	0.25	0.00	−0.02	$P_{1,0}$
A	1399.27	(020)	0.51	0.02	−0.02	$P_{2,0}$
A	2094.99	(030)	0.76	0.06	0.00	$P_{3,0}$
A	2787.9	(040)	0.88	−0.02	−0.10	$P_{4,0}$
A	3478.	(050)	0.9	−0.14	−0.24	$P_{5,0}$
RMS			0.71	0.07	0.12	
Mean			0.66	−0.02	−0.08	
Stretching polyads						
B	1042.08	(001)	0.53	0.34	0.09	$P_{0,1}$
A	1103.14	(100)	0.01	−0.20	−0.24	$P_{0,1}$
A	2057.89	(002)	1.01	0.58	0.27	$P_{0,2}$
B	2110.78	(101)	0.16	−0.27	−0.48	$P_{0,2}$
A	2201.16	(200)	0.23	−0.16	−0.23	$P_{0,2}$
B	3046.09	(003)	1.21	0.58	0.30	$P_{0,3}$
A	3083.70	(102)	0.10	−0.54	−0.74	$P_{0,3}$
B	3186.41	(201)	0.54	−0.07	−0.29	$P_{0,3}$
A	3289.93	(300)	0.42	−0.12	−0.18	$P_{0,3}$
A	4001.31	(004)	0.78	0.01	−0.18	$P_{0,4}$
B	4021.85	(103)	−0.26	−1.05	−1.18	$P_{0,4}$
A	4141.42	(202)	1.16	0.37	0.17	$P_{0,4}$
B	4250.22	(301)	0.56	−0.19	−0.36	$P_{0,4}$
A	4370.3	(400)	1.0	0.40	0.36	$P_{0,4}$
RMS			0.70	0.44	0.45	
Mean			0.54	−0.02	−0.19	
Mixed bending-stretching polyads						
B	1726.52	(011)	0.82	0.42	0.15	$P_{1,1}$
A	1796.26	(110)	0.21	−0.23	−0.29	$P_{1,1}$
B	2407.94	(021)	1.11	0.51	0.23	$P_{1,1}$
A	2486.58	(120)	0.40	−0.24	−0.33	$P_{2,1}$
A	2726.11	(012)	1.33	0.74	0.41	$P_{1,2}$
B	2785.24	(111)	0.36	−0.26	−0.49	$P_{1,2}$
A	2886.18	(210)	0.37	−0.22	−0.31	$P_{1,2}$
B	3086.22	(031)	1.40	0.63	0.33	$P_{3,1}$
A	3173.93	(130)	0.57	−0.25	−0.36	$P_{3,1}$
A	3390.92	(022)	1.65	0.90	0.58	$P_{2,2}$
B	3455.82	(121)	0.54	−0.24	−0.48	$P_{2,2}$
A	3568.07	(220)	0.51	−0.27	−0.38	$P_{2,2}$
B	3698.29	(013)	1.55	0.78	0.50	$P_{1,3}$
A	3739.43	(112)	0.27	−0.51	−0.71	$P_{1,3}$
B	3849.91	(211)	0.66	−0.10	−0.33	$P_{1,3}$
A	3859.	(140)	1.64	0.65	0.53	$P_{4,1}$
RMS			0.98	0.49	0.42	
Mean			0.84	0.14	−0.06	
Total						
RMS			0.84	0.43	0.41	
Mean			0.69	0.05	−0.12	

[a] Symmetry type of the upper vibrational state. [b] Observed centers for rovibrational bands ($v_1v_2v_3$) – (000), collected in (ref. 12, 22, 25, 26 and references therein) up to 4300 cm^{-1}. [c] ($v_1v_2v_3$) – normal mode vibrational quantum numbers. [d] Discrepancies between observed band centers and those calculated using the currently most accurate BO PES of ref. 12. [e] Discrepancies between observed band centers and those computed with DBOC corrections using CAS(n,n). All values are in cm^{-1}.

Table 4 Observed–calculated statistics for vibrational polyads of $^{16}O_3$ isotopologue at various levels of *ab initio* theory

		RMS (observed–calculated)			Mean (observed–calculated)		
Polyad	E_p [a]	BO[b]	DBOC(4,4)	DBOC(6,6)	BO[b]	DBOC(4,4)	DBOC(6,6)
$P_{1,0}$	700.93	0.25	0.00	0.02	0.25	0.00	−0.02
$P_{0,1}$	1072.61	0.38	0.28	0.18	0.28	0.07	−0.08
$P_{2,1}$	1399.27	0.51	0.02	0.02	0.51	0.02	−0.02
$P_{1,1}$	1761.39	0.60	0.33	0.23	0.52	0.09	−0.07
$P_{3,0}$	2094.99	0.77	0.06	0.00	0.77	0.06	0.00
$P_{0,2}$	2123.28	0.60	0.38	0.35	0.47	0.05	−0.15
$P_{2,1}$	2447.26	0.84	0.40	0.28	0.76	0.13	−0.05
$P_{4,0}$	2787.90	0.88	0.02	0.10	0.88	−0.02	−0.10
$P_{1,2}$	2799.17	0.83	0.47	0.41	0.69	0.09	−0.13
$P_{3,1}$	3130.07	1.07	0.48	0.35	0.99	0.19	−0.02
$P_{0,3}$	3151.53	0.70	0.40	0.44	0.57	−0.04	−0.23
$P_{2,2}$	3471.60	1.05	0.56	0.49	0.91	0.13	−0.09
$P_{5,0}$	3478.00	0.91	0.14	0.24	0.91	−0.14	−0.24
$P_{1,3}$	3813.58	0.89	0.48	0.48	0.75	−0.01	−0.21
$P_{4,1}$	3859.00	1.64	0.65	0.53	1.64	0.65	0.53
$P_{0,4}$	4157.02	0.83	0.54	0.58	0.66	−0.09	−0.24
$P_{3,2}$	4184.38	0.86	0.15	0.32	0.85	−0.07	−0.26
$P_{2,3}$	4346.73	1.86	0.97	0.71	1.86	0.97	0.71

All values are in cm^{-1}. [a] Mean value of the vibrational energy of a given polyad, including all the experimentally known levels of Table 3 with the same notations. [b] As computed with the most accurate to date *ab initio* BO PES.[12]

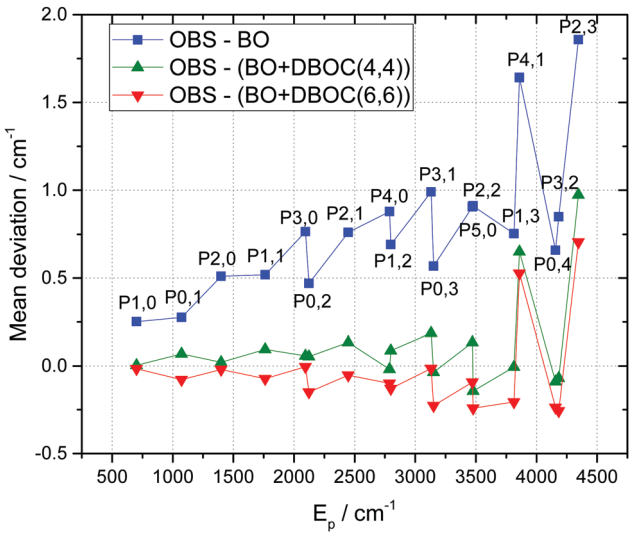

Fig. 5 Mean energy deviations for successive vibrational $P_{b,s}$ polyads of $^{16}O_3$ between observations (OBS) and the *ab initio* calculation (vertical scale) *versus* the average polyad energies (E_P, on the horizontal scale). Blue line: BO approximation,[12] green line: BO + DBOC(4,4) and red line: BO + DBOC(6,6).

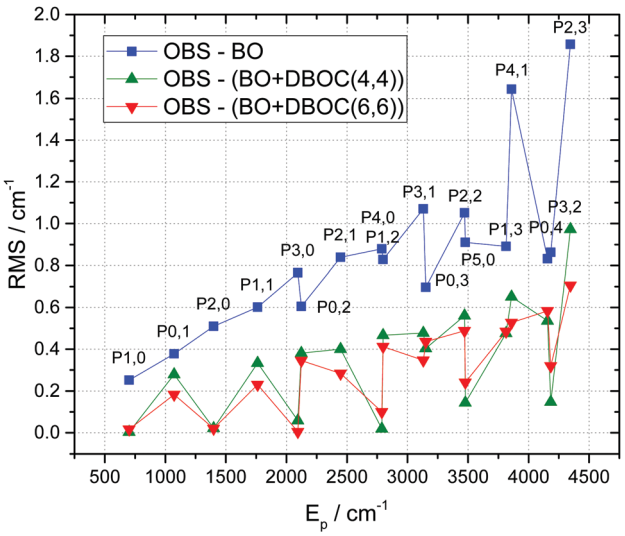

Fig. 6 Root-mean-squares (RMS) energy deviations for successive vibrational $P_{b,s}$ polyads of $^{16}O_3$ between observations (OBS) and the *ab initio* calculation (vertical scale) *versus* the average polyad energies (E_P, on the horizontal scale). Blue line: BO approximation,[12] green line: BO + DBOC(4,4) and red line: BO + DBOC(6,6).

accuracy as shown in Fig. 7. Note, that higher very weak bending bands $4\nu_2$ and $5\nu_2$ have not been directly observed. The corresponding vibrational states (040) and (050) were considered in experimental analysis of the spectra as "dark" ones[3] and have been evaluated indirectly[90] from resonance perturbations of certain rovibrational transitions. The experimental accuracy for these "dark" states roughly corresponds to the number of digits given in the first column of Table 3. Consequently, a part of the (observed–calculated) deviations for (040) and (050) have to be attributed to the experimental uncertainty. The same comments apply to other vibrational states that have been considered as "dark" ones in experimental spectral analyses. This is the case of (400) and (140) in Table 3, for which we give only one decimal digit for the virtually "observed" values. In such cases, the (observed–calculated) deviations can be impacted by experimental uncertainties.

For a general view on the energy contributions involving stretching bands we plot in Fig. 8 and 9 the mean and RMS (observed–calculated) deviations for the G_s band systems where $s = v_1 + v_3$ is a total stretching quantum number. Here the G_s band system gathers all $P_{b,s}$ polyads with various bending quantum numbers $b = v_2$ using the same cut-off as in Tables 3 and 4:

$$G_0 = \cup\{(0b0)\},\ G_1 = \cup\{(1b0),(0b1)\},$$
$$G_2 = \cup\{(2b0),(1b1),(0b2)\},\ldots,G_s = \cup\{P_{b,s}\}, \quad (6)$$

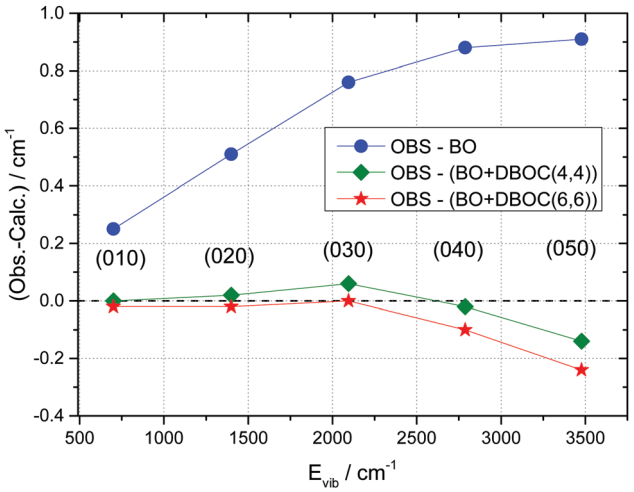

Fig. 7 Energy deviations between observations and the *ab initio* calculation (vertical scale) *versus* the vibrational energy (E_{vib}) for the bending states of $^{16}O_3$. Blue line: BO approximation,[12] green line: BO + DBOC(4,4), and red line: BO + DBOC(6,6).

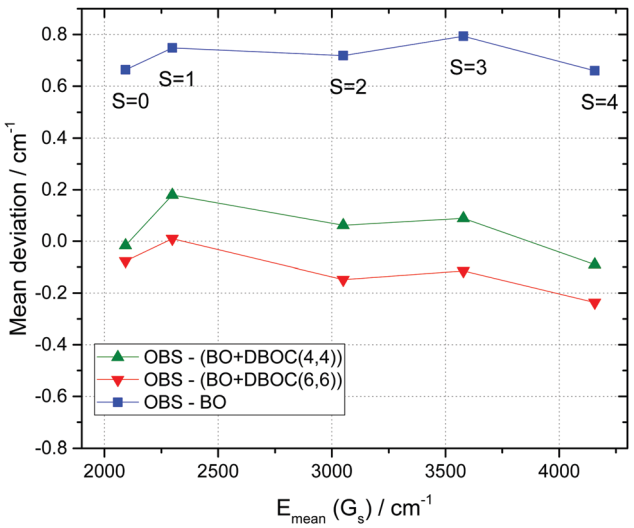

Fig. 8 Mean energy deviations for G_s groups (eqn (6)) of vibrational levels of $^{16}O_3$ between observations and *ab initio* calculations (vertical scale) with the increasing total stretching quantum number *s*. The average G_s energies are given at the horizontal scale. Blue line: BO approximation,[12] green line: BO + DBOC(4,4), and red line: BO + DBOC(6,6).

where the $\cup$ symbol stands for a union over all $b = v_2$ values included in Tables 3 and 4. The mean vibrational energy of the G_s groups of levels denoted as $E_{mean}(G_s)$ is shown along the horizontal scales of Fig. 8 and 9, in cm^{-1}.

In a sense, these plots of Fig. 8 and 9 give hints concerning the errors of the calculation averaged over bending quantum numbers as a function of excitations of the stretching vibrational modes. Again, it is seen that the inclusion of the adiabatic corrections globally improves the set of stretching vibrational levels for the considered energy cut-off. The BO + DBOC(4,4) and BO + DBOC(6,6) show again very similar performance with the average (observed–calculated) discrepancies below 0.5 cm^{-1}.

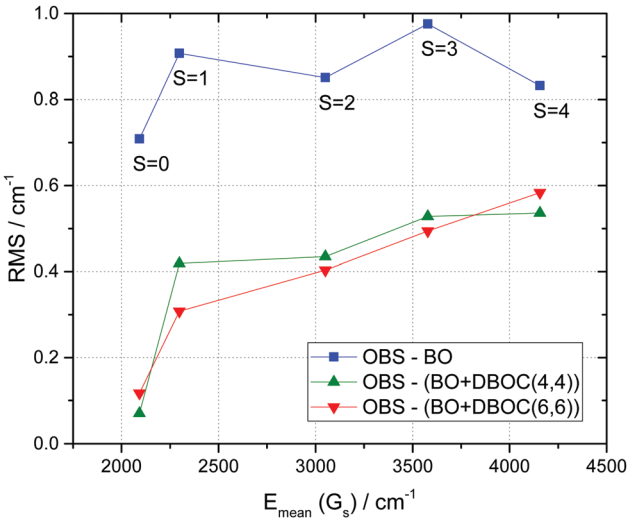

Fig. 9 Root-mean-squares (RMS) energy deviations for G_s groups (eqn (6)) of vibrational levels of $^{16}O_3$ between observations and *ab initio* calculations (vertical scale) with the increasing total stretching quantum number *s*. The average G_s energies are given at the horizontal scale. Blue line: BO approximation,[12] green line: BO + DBOC(4,4), and red line: BO + DBOC(6,6).

5 *Ab initio* vibrational energy levels of $^{18}O_3$ and $^{17}O_3$ isotopologues with DBOC corrections

As the next step of this work, let us now examine the mass dependence of the DBOC corrections in vibrational levels for the homogeneous isotopic substitutions $^{18}O_3$ and $^{17}O_3$. Experimental spectra of $^{18}O_3$ have been recorded and analyzed in a series of works (see ref. 26, 91–94, and references therein). There are significantly less observed bands than for the main ozone species, but the general trends in the improvement of the calculations are quite similar. For this reason, we only quote in this case the (observed–calculated) values and statistics at our highest level DBOC calculations using CAS(6,6). The comparisons with the observed band centers are presented in Tables 5 and 6, as well as in Fig. 10–13. As for $^{16}O_3$, we obtain the most pronounced improvement for the bending states – by more than an order of magnitude – even though the observed series is much shorter, limited here to the ν_2 and $2\nu_2$ bands. The inclusion of DBOC corrections also permitted significantly more accurate results for mixed bending-stretching polyads: the RMS (observed–calculated) deviation drops down from 0.93 cm^{-1} to 0.39 cm^{-1}, while the mean (observed–calculated) deviation is reduced from 0.77 cm^{-1} to no more than 0.04 cm^{-1}. For pure stretching polyads the improvement is less pronounced, possibly because the errors obtained with the BO PES[12] in the v_1 band and in the combination series $v_1 + nv_3$ were already very small (between 0.02 cm^{-1} to 0.2 cm^{-1}). This applies for $^{16}O_3$, $^{18}O_3$ and $^{17}O_3$ species as well. However, the general trend in improvement of the total (observed–calculated) statistics is clearly confirmed by the reported comparisons for all three isotopologues.

Table 5 Comparison of vibrational band centers computed from BO and BO + DBOC(6,6) *ab initio* potential energy surfaces with experimental data for the $^{18}O_3$ ozone isotopologue

T[a]	O = Obs.[b]	$(v_1v_2v_3)$[c]	O-BO[d]	O-DBOC(6,6)[e]	Polyad
Bending states					
A	661.49	(010)	0.21	−0.02	$P_{1,0}$
A	1320.70	(020)	0.44	−0.01	$P_{2,0}$
RMS			0.34	0.02	
Mean			0.33	−0.01	
Stretching polyads					
B	984.82	(001)	0.48	0.10	$P_{0,1}$
A	1041.56	(100)	0.02	−0.20	$P_{0,1}$
A	1946.46	(002)	0.93	0.28	$P_{0,2}$
B	1995.97	(101)	0.14	−0.42	$P_{0,2}$
A	2078.37	(200)	0.20	−0.20	$P_{0,2}$
B	2883.86	(003)	1.14	0.34	$P_{0,3}$
A	2919.96	(102)	0.11	−0.64	$P_{0,3}$
B	3012.54	(201)	0.45	−0.27	$P_{0,3}$
B	3813.41	(103)	0.19	−1.02	$P_{0,4}$
B	4019.29	(301)	0.48	−0.33	$P_{0,4}$
RMS			0.54	0.46	
Mean			0.38	−0.24	
Mixed bending-stretching polyads					
B	1631.72	(011)	0.73	0.15	$P_{1,1}$
A	1696.17	(110)	0.18	−0.25	$P_{1,1}$
B	2275.97	(021)	0.97	0.22	$P_{2,1}$
A	2348.33	(120)	0.35	−0.28	$P_{2,1}$
A	2578.99	(012)	1.22	0.41	$P_{1,2}$
B	2634.24	(111)	0.32	−0.41	$P_{1,2}$
A	2725.88	(210)	0.33	−0.27	$P_{1,2}$
B	3269.22	(121)	0.47	−0.42	$P_{2,2}$
B	3502.23	(013)	1.45	0.52	$P_{1,3}$
B	4117.32	(023)	1.72	0.70	$P_{2,3}$
RMS			0.93	0.39	
Mean			0.77	0.04	
Total					
RMS			0.73	0.41	
Mean			0.55	−0.09	

[a] Symmetry type of the upper vibrational state. [b] Observed centers for rovibrational bands $(v_1v_2v_3)$ – (000), collected in (ref. 26, 91–94 and references therein) up to 4300 cm^{-1}. [c] $(v_1v_2v_3)$ – normal mode vibrational quantum numbers. [d] Discrepancies between observed band centers and those calculated using the currently most accurate BO PES of ref. 12. [e] Discrepancies between observed band centers and those computed with DBOC corrections using CAS(n,n). All values are in cm^{-1}.

Table 6 Observed–calculated statistics for *ab initio* calculations of vibrational polyads of the $^{18}O_3$ isotopologue including DBOC corrections

		RMS (observed–calculated)		Mean (observed–calculated)	
Polyad	E_p[a]	BO[b]	DBOC(6,6)	BO[b]	DBOC(6,6)
$P_{1,0}$	661.49	0.21	0.01	0.21	−0.01
$P_{0,1}$	1013.19	0.34	0.16	0.25	−0.06
$P_{2,0}$	1320.70	0.44	0.01	0.44	−0.01
$P_{1,1}$	1663.94	0.53	0.21	0.45	−0.05
$P_{0,2}$	2006.93	0.55	0.31	0.42	−0.11
$P_{2,1}$	2312.15	0.73	0.25	0.66	−0.03
$P_{1,2}$	2646.37	0.75	0.37	0.62	−0.09
$P_{0,3}$	2938.79	0.71	0.44	0.57	−0.19
$P_{2,2}$	3269.22	0.47	0.41	0.47	−0.41
$P_{1,3}$	3502.23	1.45	0.52	1.45	0.52
$P_{0,4}$	3916.35	0.36	0.76	0.14	−0.68
$P_{2,3}$	4117.32	1.72	0.70	1.72	0.70

All values are in cm^{-1}. [a] Mean value of the vibrational energy of a given polyad, including all the experimentally known levels of Table 5 with the same notations. [b] As computed with the most accurate to date *ab initio* BO PES.[12]

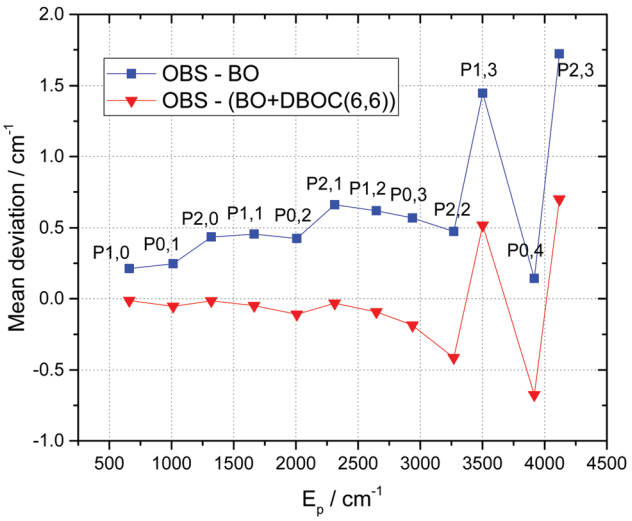

Fig. 10 Mean energy deviations for successive vibrational $P_{b,s}$ polyads of $^{18}O_3$ between observations and *ab initio* calculation (vertical scale) *versus* average polyad energies (E_P, on the horizontal scale). Values for both axes are given in cm^{-1}. Blue line: BO approximation,[12] and red line: BO + DBOC(6,6).

For the rare $^{17}O_3$ isotopologue only four centers of stretching bands have been deduced from analyses of experimental spectra in ref. 27 and 95. Again, we obtained an improvement for the RMS and mean (observed–calculated) values by accounting for the DBOC corrections as given in Table 7.

6 Discussion and conclusions

In this work, we computed mass-dependent diagonal Born–Oppenheimer corrections to the *ab initio* electronic ground state potential energy surface for the main $^{16}O_3$ isotopologue of the ozone molecule, as well as for homogeneous isotopic substitutions $^{17}O_3$ and $^{18}O_3$, which had not been investigated previously. The goal was to improve the accuracy of the PES with respect to the currently best results for vibrational states obtained in the BO approximation,[12] which was on average about 0.5 cm^{-1} for low vibrations and about 1 cm^{-1} for the entire set of observed bands. The other objective was to investigate the mass-dependence of the PESs in the $^{16}O_3$, $^{17}O_3$, and $^{18}O_3$ isotopic series and the corresponding impact on vibrational states. As the ozone molecule is known to be a strongly multireference system, we used to this end an MR-CISD ansatz in the MRCC program with CAS(4,4) and CAS(6,6) actives spaces. The DBOC contributions to electronic energies were then fitted to an analytical form in terms of nuclear displacements from the equilibrium. Finally, the vibrational band centers were computed using the nuclear motion variational method using

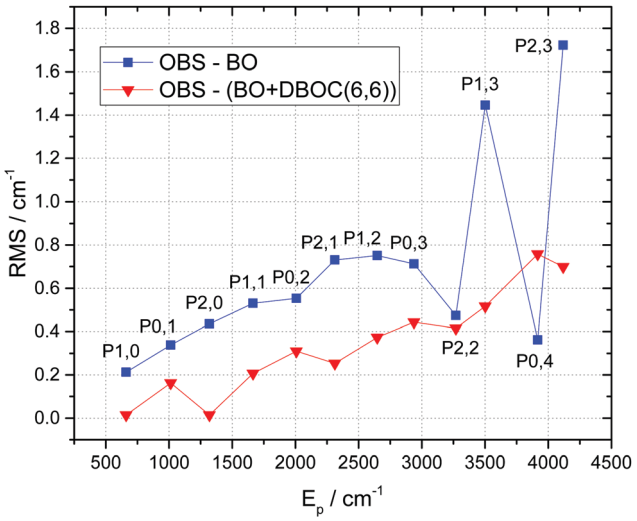

Fig. 11 Root-mean-squares (RMS) deviation between observed $^{18}O_3$ polyads and *ab initio* calculations (vertical scale) *versus* mean values E_P of vibrational $P_{b,s}$ polyads (horizontal scale). Values for both axes are given in cm^{-1}. Blue line: BO approximation,[12] and red line: BO + DBOC(6,6).

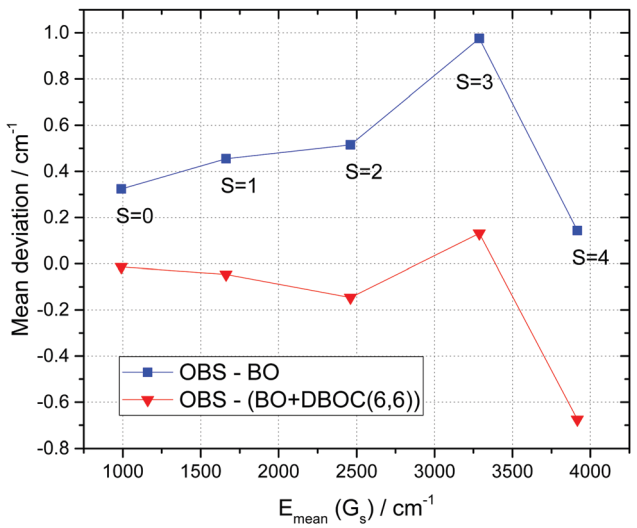

Fig. 12 Mean energy deviations for G_s groups (eqn (6)) of vibrational levels of $^{18}O_3$ between observations and the *ab initio* calculation (vertical scale) with the increasing total stretching quantum number *s*. The average G_s energies are given on the horizontal scale. Blue line: BO approximation,[12] and red line: BO + DBOC(6,6).

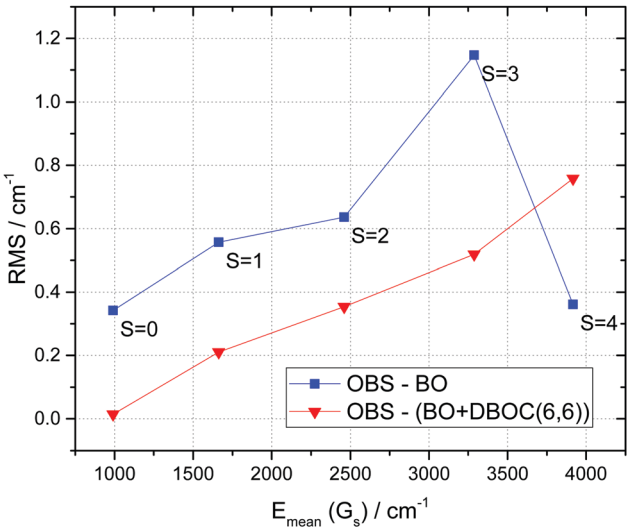

Fig. 13 Root-mean-squares (RMS) energy deviations for G_s groups (eqn (6)) of vibrational levels of $^{18}O_3$ between observations and *ab initio* calculations (vertical scale) with the increasing total stretching quantum number *s*. The average G_s energies are given on the horizontal scale. Blue line: BO approximation,[12] and red line: BO + DBOC(6,6).

Table 7 Comparison of vibrational band centers computed from BO and BO + DBOC(6,6) *ab initio* potential energy surfaces with experimental data for the $^{17}O_3$ ozone isotopologue

T[a]	O = Obs.[b]	$(v_1v_2v_3)$[c]	O-BO[d]	O-DBOC(6,6)[e]	Polyad
Bending states					
B	1012.16	(001)	0.50	0.09	$P_{0,1}$
A	1070.95	(100)	0.02	−0.22	$P_{0,1}$
A	1999.56	(002)	0.83	0.14	$P_{0,2}$
B	2050.82	(101)	0.16	−0.44	$P_{0,2}$
RMS			0.49	0.26	
Mean			0.38	−0.11	

[a] Symmetry type of the upper vibrational state. [b] Observed centers for rovibrational bands $(v_1v_2v_3)$ – (000), from ref. 27 and 95 up to 4300 cm^{-1}. [c] $(v_1v_2v_3)$ – normal mode vibrational quantum numbers. [d] Discrepancies between observed band centers and those calculated using the currently most accurate BO PES of ref. 12. [e] Discrepancies between observed band centers and those computed with DBOC corrections using CAS(*n*,*n*). All values are in cm^{-1}.

the BO + DBOC PESs for the three species and compared to available experimental values. The focus of this work was the energy range of up to about $D_0/2$ – half of the dissociation threshold – for the reasons explained in Sections 2 and 3 and summarized below. The conclusions are the following. The DBOC corrections in all the considered CAS versions produced positive contributions to vibrational energies, which are quite similar for $^{16}O_3$, $^{17}O_3$ and $^{18}O_3$ ranging from 0.3 cm^{-1} up to 1.1 cm^{-1} and gradually increasing in absolute values with increasing number of vibrational quanta. The comparison with experimental band centers shows a significant improvement of the accuracy with respect to the best BO calculations. For the low vibrational range the BO calculations of ref. 12 using atomic masses were generally slightly underestimated with positive (observed–calculated) deviations. The DBOC(4,4) and DBOC(6,6) corrections modify this in the right direction, providing a remarkable reduction in the errors of the calculation as is clearly seen in Tables 3 and 4 and on Fig. 7–9. The account of DBOC produces the most pronounced improvement for bending states and for mixed bending-stretching polyads. In the case of (010), (020) and (030) states the errors are reduced by more than one order of magnitude: the (observed–calculated) deviation for BO + DBOC(6,6) is below 0.02 cm^{-1} (Fig. 7 and Table 3), approaching nearly the experimental accuracy. Similar improvement occurs for the bending states of $^{18}O_3$ (Table 5). For combination states with three vibrational quanta, the DBOC corrections bring

ab initio calculations to the mean errors below 0.2 cm^{-1} as shown in Tables 3–6 and Fig. 5–13. To our knowledge, this level of *ab initio* accuracy has not been obtained so far for molecules with such a complex multireference electronic structure as ozone. Note that DBOC(4,4) appears to be competitive with DBOC(6,6) and provides even slightly better results for some polyad series. Possibly, the convergence with respect to the size of the CAS in the considered energy range was approached. Let us remember, however, that full variational electronic energy calculations with the triple-ζ quality basis set were only performed with the the CAS(4,4) space. CAS(6,6) calculations were only possible using an approximate incremental scheme (eqn (2)) using a double-ζ basis set, a novel approach clearly justified by the results. It is curious to note in Fig. 5 and 8 that the mean (observed–calculated) deviations would tend to almost zero values if one takes the average of DBOC(4,4) and DBOC(6,6) – green and red lines in Fig. 5 and 8 – which, although possibly no more than a fortunate coincidence, can be interpreted as a hint that the incremental formulation defined in eqn (2) might be overestimating the effect of the larger CAS to a certain extent.

Anyway, in terms of the mean (observed–calculated) deviations, the improvement is quite striking. In total, they drop down from 0.69 cm^{-1} (BO) to 0.05 cm^{-1} (DBOC(4,4)) or to 0.12 cm^{-1} (DBOC(6,6)) for the considered range including the set of $^{16}O_3$ vibrations in Table 3 with five bending and four stretching quanta. For $^{18}O_3$, the mean (observed–calculated) deviations drop down from 0.55 cm^{-1} (BO) to −0.09 cm^{-1} (DBOC(6,6)). This means that DBOC corrections almost remove the systematic BO errors in vibrational levels below $E_{BO} = D_0/2$. The remaining (observed–calculated) scattering naturally increases with energy that could be attributed to both BO and to DBOC uncertainties in the analytical models, as well as to individual vibrational modes. However, the DBOC corrections generally reduce the total RMS (observed–calculated) deviations by a factor of two or so: from 0.84 cm^{-1} to 0.41 cm^{-1} for $^{16}O_3$, from 0.73 cm^{-1} to 0.41 cm^{-1} for $^{18}O_3$ and from 0.49 cm^{-1} to 0.26 cm^{-1} for $^{17}O_3$. The present results, including the full sets of calculated vibrational states provided in the ESI† with (observed–calculated) statistics, can be used for improving the effective spectroscopic models for analyses of observations. The Fortran code for the BO PES[12] is available in the S&MPO ("Spectroscopy and Molecular Properties of Ozone") database and information system,[26] while the Python code for the DBOC correction surface and calculated vibrational levels are provided in the ESI† of this paper.

Despite significant progress,[3,26] some ozone bands below $E_{BO} = D_0/2$ have not yet been fully analyzed. For complicated coupled band systems belonging to overlapping polyads,[96] *ab initio* values are often used for constraining parameters, which are missing from direct measurements. Typically, "dark" states are fixed to theoretically predicted values. Their accuracy has thus a considerable impact on spectral perturbations induced by accidental rovibrational Coriolis or Darling–Dennison resonances.[3,25,26,85] This is particularly important for rare species like $^{18}O_3$ and $^{17}O_3$, where much fewer spectral assignments are yet available. As explained in Sections 2 and 3, reliable DBOC calculations with the targeted accuracy were possible to carry out up to about half of the dissociation threshold – at least using the currently feasible *ab initio* ansatz with accessible computational facilities. Above this energy corresponding to ≈4300 cm^{-1}, *ab initio* calculations were not well converged for certain nuclear geometries and/or the fits to analytic models yielded erratic series with outliers much larger than 1 cm^{-1} despite the use of several trial functions. Although this could potentially happen due to an insufficiently large active space or a too low cardinal number for the atomic basis set, we consider the limitation to the use of single reference Hartree–Fock Self-Consistent-Field orbitals in the DBOC calculations as the major obstacle to achieving higher accuracy. Note that the most accurate to date BO PES,[12] which we used in this work, had been constructed using CAS(18,12) with complete active space self-consistent field (CASSCF) orbitals in the $X = 5,6 \rightarrow \infty$ extrapolated complete basis set limit. In addition, it accounted for a supplementary correction[12] due to a simultaneous optimization of 13 excited electronic states considered by Dawes *et al.*,[10] which had a significant impact on the shape of the PES[10,11,14] and the dynamics[35,37,38] in the range near the transition state towards the dissociation. Another challenge is to account for non-adiabatic interactions among 27 electronic states corresponding to the same dissociation limit[39,97] and for possible effects of the topological phase[8] related to conical intersections.[40] At a high energy range, the effects of the delocalization of the vibrational state wave functions among three potential wells also have to be accounted for.[98] However, the reported results at the present state of the art already provide an encouraging accuracy validation for the multireference methods of the *ab initio* theory, at least in the range of up to four vibrational quanta. In future works, we plan to address the above issues, as well as to extend DBOC calculations to non-homogeneous isotopic species of ozone.

Conflicts of interest

The authors declare no conflicts of interest.

Acknowledgements

This work has been supported by the Russian Science Foundation RNF grant no. 19-12-00171. A. T. acknowledges the support from CNRS for the research stay at Reims University.

References

1 R. Siebert, P. Fleurat-Lessard, R. Schinke, M. Bittererová and S. C. Farantos, *J. Chem. Phys.*, 2002, **116**, 9749–9767.
2 J.-M. Flaud and J. Orphal, *Handbook of High-resolution Spectroscopy*, John Wiley & Sons, Ltd, Chichester, UK, 2011.
3 A. Barbe, S. Mikhailenko, E. Starikova, M.-R. De Backer, V. Tyuterev, D. Mondelain, S. Kassi, A. Campargue, C. Janssen, S. Tashkun, R. Kochanov, R. Gamache and J. Orphal, *J. Quant. Spectrosc. Radiat. Transfer*, 2013, **130**, 172–190.

4 L. Costantino, J. Cuesta, E. Emili, A. Coman, G. Foret, G. Dufour, M. Eremenko, Y. Chailleux, M. Beekmann and J.-M. Flaud, *Atmos. Meas. Tech.*, 2017, **10**, 1281–1298.
5 S. S. Xantheas, G. J. Atchity, S. T. Elbert and K. Ruedenberg, *J. Chem. Phys.*, 1991, **94**, 8054–8069.
6 A. Banichevich, S. D. Peyerimhoff and F. Grein, *Chem. Phys.*, 1993, **178**, 155–188.
7 T. Müller, S. S. Xantheas, H. Dachsel, R. J. Harrison, J. Nieplocha, R. Shepard, G. S. Kedziora and H. Lischka, *Chem. Phys. Lett.*, 1998, **293**, 72–80.
8 P. Garcia-Fernandez, I. B. Bersuker and J. E. Boggs, *Phys. Rev. Lett.*, 2006, **96**, 163005.
9 F. Holka, P. G. Szalay, T. Müller and V. G. Tyuterev, *J. Phys. Chem. A*, 2010, **114**, 9927–9935.
10 R. Dawes, P. Lolur, J. Ma and H. Guo, *J. Chem. Phys.*, 2011, **135**, 18–22.
11 V. G. Tyuterev, R. Kochanov, A. Campargue, S. Kassi, D. Mondelain, A. Barbe, E. Starikova, M. R. De Backer, P. G. Szalay and S. Tashkun, *Phys. Rev. Lett.*, 2014, **113**, 143002.
12 V. G. Tyuterev, R. V. Kochanov, S. A. Tashkun, F. Holka and P. G. Szalay, *J. Chem. Phys.*, 2013, **139**, 134307.
13 M. Ayouz and D. Babikov, *J. Chem. Phys.*, 2013, **138**, 164311.
14 R. Dawes, P. Lolur, A. Li, B. Jiang and H. Guo, *J. Chem. Phys.*, 2013, **139**, 201103.
15 S. Y. Grebenshchikov, Z.-W. Qu, H. Zhu and R. Schinke, *Phys. Chem. Chem. Phys.*, 2007, **9**, 2044.
16 K. Mauersberger, *Geophys. Res. Lett.*, 1981, **8**, 935–937.
17 M. H. Thiemens and J. E. Heidenreich, *Science*, 1983, **219**, 1073–1075.
18 K. Mauersberger, B. Erbacher, D. Krankowsky, J. Günther and R. Nickel, *Science*, 1999, **283**, 370–372.
19 H. Hippler, R. Rahn and J. Troe, *J. Chem. Phys.*, 1990, **93**, 6560–6569.
20 C. Janssen, J. Guenther, D. Krankowsky and K. Mauersberger, *Chem. Phys. Lett.*, 2003, **367**, 34–38.
21 M. H. Thiemens, *Proc. Natl. Acad. Sci. U. S. A.*, 2013, **110**, 17631–17637.
22 V. Tyuterev, S. Tashkun, P. Jensen, A. Barbe and T. Cours, *J. Mol. Spectrosc.*, 1999, **198**, 57–76.
23 S. Ndengué, R. Dawes, X. G. Wang, T. Carrington, Z. Sun and H. Guo, *J. Chem. Phys.*, 2016, **144**, 074302.
24 D. Lapierre, A. Alijah, R. Kochanov, V. Kokoouline and V. Tyuterev, *Phys. Rev. A*, 2016, **94**, 042514.
25 J. Flaud and R. Bacis, *Spectrochim. Acta, Part A*, 1998, **54**, 3–16.
26 Y. L. Babikov, S. N. Mikhailenko, A. Barbe and V. G. Tyuterev, *J. Quant. Spectrosc. Radiat. Transfer*, 2014, **145**, 169–196.
27 D. Consalvo, A. Perrin, J. Flaud, C. Camypeyret, A. Valentin and C. Chardonnet, *J. Mol. Spectrosc.*, 1994, **168**, 92–98.
28 E. Starikova, A. Barbe, M.-R. De Backer-Barilly, V. Tyuterev, S. Tashkun, S. Kassi and A. Campargue, *Chem. Phys. Lett.*, 2009, **470**, 28–34.
29 D. Mondelain, A. Campargue, S. Kassi, A. Barbe, E. Starikova, M.-R. De Backer and V. G. Tyuterev, *J. Quant. Spectrosc. Radiat. Transfer*, 2013, **116**, 49–66.
30 V. G. Tyuterev, A. Barbe, D. Jacquemart, C. Janssen, S. N. Mikhailenko and E. N. Starikova, *J. Chem. Phys.*, 2019, **150**, 184303.
31 E. Starikova, A. Barbe and V. G. Tyuterev, *J. Quant. Spectrosc. Radiat. Transfer*, 2019, **232**, 87–92.
32 R. Schinke, S. Y. Grebenshchikov, M. Ivanov and P. Fleurat-Lessard, *Annu. Rev. Phys. Chem.*, 2006, **57**, 625–661.
33 C. A. M. Brenninkmeijer, C. Janssen, J. Kaiser, T. Röckmann, T. S. Rhee and S. S. Assonov, *Chem. Rev.*, 2003, **103**, 5125–5162.
34 A. L. Van Wyngarden, K. A. Mar, J. Quach, A. P. Q. Nguyen, A. A. Wiegel, S.-Y. Lin, G. Lendvay, H. Guo, J. J. Lin, Y. T. Lee and K. A. Boering, *J. Chem. Phys.*, 2014, **141**, 064311.
35 Z. Sun, D. Yu, W. Xie, J. Hou, R. Dawes and H. Guo, *J. Chem. Phys.*, 2015, **142**, 174312.
36 T. R. Rao, G. Guillon, S. Mahapatra and P. Honvault, *J. Phys. Chem. A*, 2015, **119**, 11432–11439.
37 G. Guillon, P. Honvault, R. Kochanov and V. Tyuterev, *J. Phys. Chem. Lett.*, 2018, **9**, 1931–1936.
38 C. H. Yuen, D. Lapierre, F. Gatti, V. Kokoouline and V. G. Tyuterev, *J. Phys. Chem. A*, 2019, **123**, 7733–7743.
39 M. Tashiro and R. Schinke, *J. Chem. Phys.*, 2003, **119**, 10186–10193.
40 A. Alijah, D. Lapierre and V. Tyuterev, *Mol. Phys.*, 2018, **8976**, 1–11.
41 M. Born and K. Huang, *Dynamical theory of crystal lattices*, Clarendon Press, Oxford, 1954.
42 H. Sellers and P. Pulay, *Chem. Phys. Lett.*, 1984, **103**, 463–465.
43 N. C. Handy, Y. Yamaguchi and H. F. Schaefer, *J. Chem. Phys.*, 1986, **84**, 4481–4484.
44 R. D. Bardo and M. Wolfsberg, *J. Chem. Phys.*, 1978, **68**, 2686–2695.
45 R. D. Bardo, L. I. Kleinman, A. W. Raczkowski and M. Wolfsberg, *J. Chem. Phys.*, 1978, **69**, 1106–1111.
46 J. O. Jensen and D. R. Yarkony, *J. Chem. Phys.*, 1988, **89**, 975–982.
47 W. Cencek and W. Kutzelnigg, *Chem. Phys. Lett.*, 1997, **266**, 383–387.
48 E. F. Valeev and C. D. Sherrill, *J. Chem. Phys.*, 2003, **118**, 3921–3927.
49 S. L. Mielke, D. W. Schwenke and K. A. Peterson, *J. Chem. Phys.*, 2005, **122**, 224313.
50 M. Przybytek and B. Jeziorski, *J. Chem. Phys.*, 2005, **123**, 134315.
51 J. Gauss, A. Tajti, M. Kállay, J. F. Stanton and P. G. Szalay, *J. Chem. Phys.*, 2006, **125**, 144111.
52 A. Tajti, P. G. Szalay and J. Gauss, *J. Chem. Phys.*, 2007, **127**, 014102.
53 J. F. Stanton, J. Gauss, L. Cheng, M. E. Harding, D. A. Matthews and P. G. Szalay, *CFOUR, Coupled-Cluster techniques for Computational Chemistry, a quantum-chemical program package*, with contributions from A. A. Auer, R. J. Bartlett, U. Benedikt, C. Berger, D. E. Bernholdt, Y. J. Bomble, O. Christiansen, F. Engel, R. Faber, M. Heckert, O. Heun, M. Hilgenberg, C. Huber, T.-C. Jagau, D. Jonsson, J. Jusélius, T. Kirsch, K. Klein, W. J. Lauderdale, F. Lipparini, T. Metzroth, L. A. Mück, D. P. O'Neill, D. R. Price, E. Prochnow, C. Puzzarini, K. Ruud, F. Schiffmann, W. Schwalbach, C. Simmons, S. Stopkowicz, A. Tajti, J. Vázquez, F. Wang, J. D. Watts and the integral packages MOLECULE (J. Almlöf and P. R. Taylor), PROPS (P. R. Taylor), ABACUS

(T. Helgaker, H. J. Aa. Jensen, P. Jørgensen, and J. Olsen), and ECP routines by A. V. Mitin and C. van Wüllen. For the current version, see http://www.cfour.de.

54 M. Kállay, P. R. Nagy, Z. Rolik, D. Mester, G. Samu, J. Csontos, J. Csóka, B. P. Szabó, L. Gyevi-Nagy, I. Ladjánszki, L. Szegedy, B. Ladóczki, K. Petrov, M. Farkas, P. D. Mezei and B. Hégely, *MRCC, a quantum chemical program suite*, See also Z. Rolik, L. Szegedy, I. Ladjánszki, B. Ladóczki and M. Kállay, *J. Chem. Phys.*, 2013, **139**, 094105, as well as: www.mrcc.hu.

55 M. Kállay and P. R. Surján, *J. Chem. Phys.*, 2001, **115**, 2945–2954.

56 M. Kállay, P. G. Szalay and P. R. Surján, *J. Chem. Phys.*, 2002, **117**, 980–990.

57 M. Kállay, J. Gauss and P. G. Szalay, *J. Chem. Phys.*, 2003, **119**, 2991–3004.

58 M. Kállay and J. Gauss, *J. Chem. Phys.*, 2004, **120**, 6841–6848.

59 P. G. Szalay, F. Holka, J. Fremont, M. Rey, K. A. Peterson and V. G. Tyuterev, *Phys. Chem. Chem. Phys.*, 2011, **13**, 3654–3659.

60 F. Holka, P. G. Szalay, J. Fremont, M. Rey, K. A. Peterson and V. G. Tyuterev, *J. Chem. Phys.*, 2011, **134**, 094306.

61 H. Partridge and D. Schwenke, *J. Chem. Phys.*, 1997, **106**, 4618–4639.

62 X. Huang, D. W. Schwenke and T. J. Lee, *J. Chem. Phys.*, 2008, **129**, 214304.

63 A. V. Nikitin, M. Rey and V. G. Tyuterev, *J. Chem. Phys.*, 2016, **145**, 114309.

64 A. Owens, S. N. Yurchenko, A. Yachmenev, J. Tennyson and W. Thiel, *J. Chem. Phys.*, 2016, **145**, 104305.

65 A. Tajti, P. G. Szalay, A. G. Császár, M. Kállay, J. Gauss, E. F. Valeev, B. A. Flowers, J. Vázquez and J. F. Stanton, *J. Chem. Phys.*, 2004, **121**, 11599–11613.

66 Y. J. Bomble, J. Vázquez, M. Kállay, C. Michauk, P. G. Szalay, A. G. Császár, J. Gauss and J. F. Stanton, *J. Chem. Phys.*, 2006, **125**, 064108.

67 M. E. Harding, J. Vázquez, B. Ruscic, A. K. Wilson, J. Gauss and J. F. Stanton, *J. Chem. Phys.*, 2008, **128**, 114111.

68 J. H. Thorpe, C. A. Lopez, T. L. Nguyen, J. H. Baraban, D. H. Bross, B. Ruscic and J. F. Stanton, *J. Chem. Phys.*, 2019, **150**, 224102.

69 M. Heckert, M. Kállay, D. P. Tew, W. Klopper and J. Gauss, *J. Chem. Phys.*, 2006, **125**, 044108.

70 A. Karton, E. Rabinovich, J. M. L. Martin and B. Ruscic, *J. Chem. Phys.*, 2006, **125**, 144108.

71 T. Helgaker, W. Klopper and D. P. Tew, *Mol. Phys.*, 2008, **106**, 2107–2143.

72 A. Karton, *Wiley Interdiscip. Rev.: Comput. Mol. Sci.*, 2016, **6**, 292–310.

73 A. Ganyecz, M. Kállay and J. Csontos, *J. Chem. Theory Comput.*, 2017, **13**, 4193–4204.

74 C. Puzzarini, J. Bloino, N. Tasinato and V. Barone, *Chem. Rev.*, 2019, **119**, 8131–8191.

75 T. H. Dunning Jr, *J. Chem. Phys.*, 1989, **90**, 1007–1023.

76 R. A. Kendall, T. H. Dunning Jr and R. J. Harrison, *J. Chem. Phys.*, 1992, **96**, 6796–6806.

77 D. E. Woon and T. H. Dunning Jr, *J. Chem. Phys.*, 1993, **98**, 1358–1371.

78 C. Puzzarini and V. Barone, *Phys. Chem. Chem. Phys.*, 2011, **13**, 7189–7197.

79 The ROMEO HPC Center Champagne-Ardenne is an HPC platform hosted by the University of Reims Champagne-Ardenne and supported by the Champagne-Ardenne Region since 2002. See http://romeo.univ-reims.fr.

80 B. Ruscic, R. E. Pinzon, M. L. Morton, N. K. Srinivasan, M.-C. Su, J. W. Sutherland and J. V. Michael, *J. Phys. Chem. A*, 2006, **110**, 6592–6601.

81 B. Ruscic, unpublished results obtained from active thermochemical tables (ATcT) based on the Core (Argonne) Thermochemical Network version 1.110, 2010.

82 A. G. Császár, E. Mátyus, T. Szidarovszky, L. Lodi, N. F. Zobov, S. V. Shirin, O. L. Polyansky and J. Tennyson, *J. Quant. Spectrosc. Radiat. Transfer*, 2010, **111**, 1043–1064.

83 O. L. Polyansky, R. I. Ovsyannikov, A. A. Kyuberis, L. Lodi, J. Tennyson and N. F. Zobov, *J. Phys. Chem. A*, 2013, **117**, 9633–9643.

84 M. Rey, A. V. Nikitin and V. G. Tyuterev, *J. Quant. Spectrosc. Radiat. Transfer*, 2015, **164**, 207–220.

85 V. G. Tyuterev, R. V. Kochanov and S. A. Tashkun, *J. Chem. Phys.*, 2017, **146**, 064304.

86 W. Kutzelnigg, *Mol. Phys.*, 1997, **90**, 909–916.

87 K. Pachucki and J. Komasa, *J. Chem. Phys.*, 2009, **130**, 164113.

88 D. W. Schwenke, *J. Phys. Chem. A*, 2001, **105**, 2352–2360.

89 X. Huang, D. W. Schwenke, S. A. Tashkun and T. J. Lee, *J. Chem. Phys.*, 2012, **136**, 124311.

90 A. Barbe, M.-R. De Backer, E. Starikova, S. Tashkun, X. Thomas and V. Tyuterev, *J. Quant. Spectrosc. Radiat. Transfer*, 2012, **113**, 829–839.

91 A. Perrin, A.-M. Vasserot, J.-M. Flaud, C. Camy-Peyret, C. Rinsland, M. Smith and V. Malathy Devi, *J. Mol. Spectrosc.*, 1990, **143**, 311–317.

92 J.-M. Flaud, C. Camy-Peyret, V. Malathy Devi, C. Rinsland and M. Smith, *J. Mol. Spectrosc.*, 1987, **122**, 221–228.

93 A. Chichery, A. Barbe, V. Tyuterev and M. Bourgeois, *J. Mol. Spectrosc.*, 2001, **206**, 1–13.

94 A. Chichery, A. Barbe and V. Tyuterev, *J. Mol. Spectrosc.*, 2001, **206**, 14–26.

95 A. Barbe and E. Starikova, *J. Quant. Spectrosc. Radiat. Transfer*, 2019, **232**, 116–125.

96 S. Mikhailenko and A. Barbe, *J. Quant. Spectrosc. Radiat. Transfer*, 2020, **244**, 106823.

97 P. Rosmus, P. Palmieri and R. Schinke, *J. Chem. Phys.*, 2002, **117**, 4871–4877.

98 V. Kokoouline, D. Lapierre, A. Alijah and V. Tyuterev, *Phys. Chem. Chem. Phys.*, 2020, **22**, 15885–15899.